IEEE Access
Multidisciplinary ⋮ Rapid Review ⋮ Open Access Journal

Received 18 February 2023, accepted 17 March 2023, date of publication 22 March 2023, date of current version 2 May 2023.

Digital Object Identifier 10.1109/ACCESS.2023.3260218

RESEARCH ARTICLE

Analysis of Line-of-Sight Angle Characteristics for Intercepting a Non-Maneuvering Target With Impact Angle Constraints

XIN SUN[1], HUI WANG[1], KAIYANG GUO[2], YURU BIN[1], HETING WANG[1], AND KEQING GUO[1]

[1]School of Aerospace Engineering, Beijing Institute of Technology, Beijing 100081, China
[2]Beijing Institute of Electronic System Engineering, Beijing 100854, China

Corresponding author: Hui Wang (wanghuibit@bit.edu.cn)

ABSTRACT With the widespread informationization in modern warfare, higher requirements are required for monitoring the high-value target's movement state and the corresponding attack conditions. Since the impact-angle constraint guidance law can improve the striking effect of a missile, the study of the hitting conditions and corresponding angle range of the attack angle constraint guidance law has become particularly important. This paper proposes a relationship between the missile's line-of-sight and flight-path angle under terminal conditions and defines the line-of-sight selection region. Then, we analyze the selection method of the line-of-sight restriction at the end of the missile's terminal phases. Additionally, Cauchy's inequality is used to derive the mathematical expressions for line-of-sight selection region under extreme and ideal conditions when employing the developed guidance law to intercept non-maneuvering targets. Finally, a thorough analysis and numerous simulations demonstrate that the line-of-sight angle always falls within the extreme selection region during the entire flight and before hitting the target at the expected impact angle. Compared with a head-on interception, the line-of-sight selection region of the tail-chase case is broader, and the selection region range increases with the upward trend of the acceleration limit.

INDEX TERMS Impact angle constraint, line-of-sight selection region, acceleration limit, tail-chase attack, head-on interception.

I. INTRODUCTION

Intercepting moving targets at the desired impact angle is a challenging and formidable task for missiles in dynamic engagement scenarios. In the framework of realistic engagement, the missile accurately detects and intercepts the target, assisted by the seeker under certain constraints. Then, by selecting the appropriate impact angle, the missile ensures that the target does not exceed the field-of-view limit [1], [2], [3], [4]. However, the missile must intercept the target at the desired impact angle while not exceeding the available acceleration due to the available missile acceleration limitations. Therefore, the missile's and target's position restrictions and the relative motion state conditions are vital [5], [6], [7]. Nevertheless, exploring the line-of-sight angle selection region under the impact-angle control guidance law helps solve the target interception failure problem at the terminal phase due to inappropriate motion conditions [8], [9]. When the target is outside the line-of-sight angle selection region, even if the missile is guided by the maximum acceleration or a guidance law limited by the impact angle, it may not be able to intercept the target at the desired impact angle [10], [11]. Spurred by this problem, this paper explores the line-of-sight angle selection region of the guidance law while meeting the acceleration limitations and desired impact angle.

In recent years, extensive and in-depth research has been conducted on guidance laws that control the terminal impact angle and field-of-view [3], [4], [5]. For instance, [12] studied the three-dimensional nonsingular collaborative guidance law under various field-of-view limitations for multiple missiles. Moreover, [13] researched the maneuvering target interception guidance method based on virtual field-of-view limits

The associate editor coordinating the review of this manuscript and approving it for publication was Halil Ersin Soken.

and [14], [15] explored the guidance strategy considering the minimum field-of-view angle limit and the field-of-view constraint of the jet linkage seeker. In [16], the authors utilized the state-related Riccati equation to analyze the uniform applicability of impact angle control guidance, and [17] analyzed the lead-angle-based angle restriction interception. In [18] and [19], the authors studied the impact time constrained guidance law considering the field-of-view limitations.

Furthermore, the literature also focused on the guidance law in the direction of capturability and attack region. For example, [20], [21], [22], [23] analyzed the capturability in different scenarios for pure proportional guidance, true proportional guidance, and re-verse augmented proportional navigation guidance, while [24] investigated capturing the line-of-sight angle constraint guidance law of fixed targets. Mukherjee et al. [25] dis-cussed several variants of traditional cyclic pursuit and proposed an improved heterogeneous cyclic pursuit scheme to capture moving targets. Ghosh et al. [26] analyzed the capturability of augmented proportional navigation guidance for a time-varying maneuvering target. Reference [27] analyzed the field-of-view constraints' guidance capability by transforming the auxiliary variables' guidance equations. Overall, the existing literature reveals that research on the line-of-sight angle selection region guided by the impact angle constraint is rarely investigated.

Spurred by the current research gap, this study considers non-maneuvering targets and studies the line-of-sight angle selection region of the impact-angle constraint guidance law. According to the closed-loop analytical solution of the impact-angle constraint guidance law of [28], we attempt to explore the line-of-sight angle range se-lection. Specifically, this paper's main contribution is that, combined with the Cauchy inequality and trigonometric function transformation, we aim to study the influence of the impact-angle constraint guidance law on selecting the desired impact angle. Additionally, we analyze the line-of-sight angle selection region under acceleration limitations, thus providing a reference to design the guidance law.

II. PROBLEM STATEMENT

A. PROBLEM FORMULATION

Consider a planar engagement scenario, as illustrated in Fig. 1, where the target is denoted by subscript T and moves at a constant speed V_t without maneuvering. The missile is denoted by subscript M and moves toward the target with a speed of V_m. This work considers the following assumptions:

Assumption 1: The missile is faster than the target, i.e., $\eta = V_t/V_m < 1$, and the tar-get is not maneuvering.

Assumption 2: The angle of attack is small enough to be neglected.

The nonlinear engagement kinematics can be represented as:

$$\begin{cases} \dot{r} = V_t \cos(\theta_t - q) - V_m \cos\sigma \\ \dot{q} = \dfrac{V_t \sin(\theta_t - q) + V_m \sin\sigma}{r} \\ \dot{\theta}_m = a_m / V_m \end{cases} \tag{1}$$

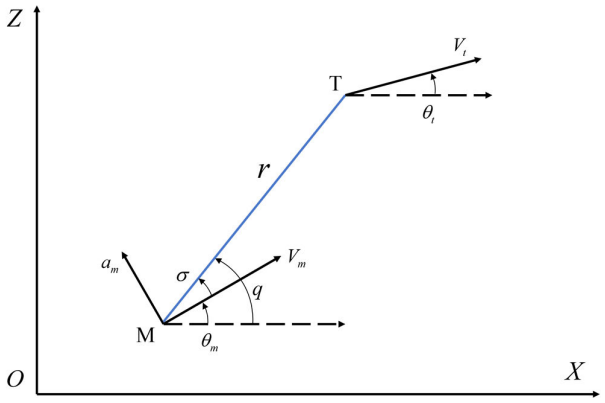

FIGURE 1. Geometry of planar motion.

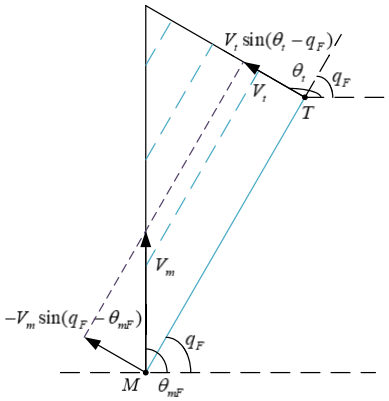

FIGURE 2. Stable collision geometry.

where r denotes the relative distance, θ_t and θ_m are the flight-path angle of the target and missile, respectively, and a_m is the missile's acceleration perpendicular to the velocity vector. The field-of-view σ is defined by rotating the angle from the di-rection of the missile velocity to the line-of-sight (LOS) angle q:

$$\sigma = q - \theta_m \tag{2}$$

In order to analyze the missile's line-of-sight angular selection range, it is essential to define interception:

Definition 1: Given an allowable miss distance R_{miss}, the target is intercepted when the range becomes less than R_{miss} at the terminal time t_F, i.e., $r\,(t_F) < R_{miss}$.

To intercept the target with a stable collision geometry, the missile and the target should form a collision route that maintains a constant LOS angle when the missile approaches the target (Figure 2).

Thus, from Eq. (1), the impact geometry constraint is [22]:

$$\eta \sin(\theta_t - q_F) + \sin(q_F - \theta_{mF}) = 0 \tag{3}$$

where q_F and θ_{mF} indicate the LOS angle and the flight-path angle of the missile at the final time, respectively. q_F is obtained from Eq. (3) by θ_{mF}, θ_{tF} and the velocity ratio η, according to the relative position relationship between the

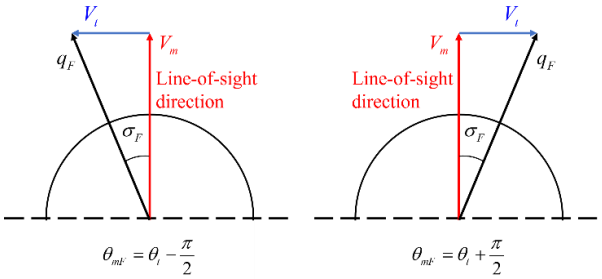

FIGURE 3. Schematic diagram of the vertical interception field-of-view at the final time.

target and missile. θ_{mF} can be expressed as:

$$\theta_{mF} = \begin{cases} q_F + \arcsin(\eta \sin(\theta_t - q_F)) \\ \quad \text{if } |q_F - \theta_{mF}| \le \pi/2 \\ q_F + \arcsin(\eta \sin(\theta_t - q_F)) - \pi \\ \quad \text{if } \left|q_f - \theta_{mF}\right| > \pi/2 \end{cases} \tag{4}$$

Considering that the seeker's field-of-view has a symmetric configuration such that $\sigma_{FOV} \in (-\sigma_{\lim}, \sigma_{\lim})$, and that typically the seeker's field-of-view range does not exceed $\pi/2$ [29], i.e., $\sigma_{\lim} < \pi/2$, Eq. (4) can be simplified to:

$$\theta_{mF} = q_F + \arcsin(\eta \sin(\theta_t - q_F)) \tag{5}$$

The missile's flight-path angle at the final time can be expressed as:

$$\theta_{mF} = \theta_t \pm \theta_e \tag{6}$$

where θ_e is the angle between the missile and the target speed directions when the missile intercepts the target. By combining Eqs. (5) and (6), the desired collision angle q_F is:

$$q_F = \begin{cases} \arctan \dfrac{\sin(\theta_t + \theta_e) - \eta \sin\theta_t}{\cos(\theta_t + \theta_e) - \eta \cos\theta_t} & \text{if } \theta_{mF} = \theta_t + \theta_e \\ \arctan \dfrac{\sin(\theta_t - \theta_e) - \eta \sin\theta_t}{\cos(\theta_t - \theta_e) - \eta \cos\theta_t} & \text{if } \theta_{mF} = \theta_t - \theta_e \end{cases} \tag{7}$$

For the particular case of vertical interception, i.e., $\theta_e = \pi/2$, and Eq, (7) can be simplified to:

$$q_F = \theta_t \pm \arctan \frac{1}{\eta} \tag{8}$$

This way, the missile's field-of-view during the terminal encounter is illustrated in Fig.3.

B. GUIDANCE LAW WITH IMPACT ANGLE CONSTRAINT

Combined with the optimal form proposed in [1] and [28], the form of the guidance law with an impact angle constraint is as follows:

$$a_c = 2(n+2)V_r\dot{q} + \frac{(n+1)(n+2)V_r(q - q_F)}{t_{go}} \tag{9}$$

where $N_1 = 2(n+2)$ is the proportional conduction factor, $N_2 = (n+1)(n+2)$ is the impact angle control gain, $\left|\vec{V}_r\right| = \left|\vec{V}_m - \vec{V}_t\right| = V_m\sqrt{1+\eta^2 - 2\eta\cos(\theta_m - \theta_t)}$ is the relative velocity between the missile and target, q_F is the desired line-of-sight angle, and t_{go} is the remaining flight time.

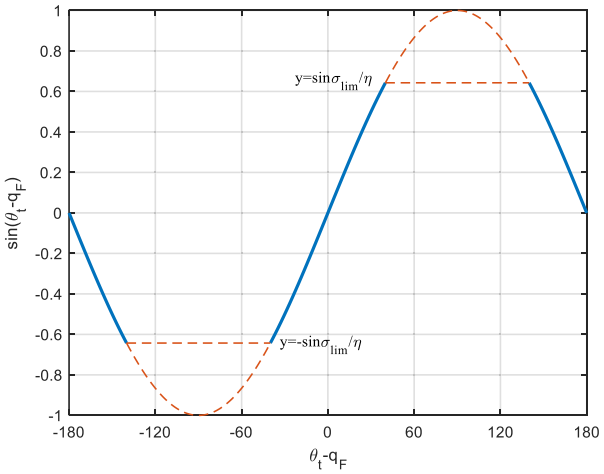

FIGURE 4. Range of the final line-of-sight (LOS) angle.

III. LINE-OF-SIGHT ANGLE SELECTION REGION ANALYSIS

A. EFFECT OF THE SEEKER FIELD-OF-VIEW RESTRICTION ON THE LINE-OF-SIGHT ANGLE AT THE FINAL TIME

When the missile enters the final guidance phase, the target falls within the seeker's field-of-view, that is, $q_0 - \theta_{m0} = \sigma_0 \in (-\sigma_{\lim}, \sigma_{\lim})$. However, due to the impact angle limitations of the final time imposed by the guidance law, to ensure that the seeker does not lose the target at the final time, we employ Eq. (5) and obtain the following:

$$\sigma_F = q_F - \theta_{mF} = -\arcsin(\eta \sin(\theta_t - q_F)) \tag{10}$$

where $\sigma_F \in (-\sigma_{\lim}, \sigma_{\lim})$.

Solving Eq. (10) yields a range of values for the impact angle under the seeker viewing angle's limitations, as presented in Eq. (11) and Fig. 4.

$$\begin{aligned} q_F \in & \left(\theta_t - \pi, \theta_t - \pi + \arcsin\left(\frac{\sin\sigma_{\lim}}{\eta}\right)\right) \\ & \cup \left(\theta_t - \arcsin\left(\frac{\sin\sigma_{\lim}}{\eta}\right), \theta_t + \arcsin\left(\frac{\sin\sigma_{\lim}}{\eta}\right)\right) \\ & \cup \left(\theta_t + \pi - \arcsin\left(\frac{\sin\sigma_{\lim}}{\eta}\right), \theta_t + \pi\right) \end{aligned} \tag{11}$$

To ensure that the missile does not lose the target at the final time when the speed ratio of the target and missile is satisfied with the seeker's field-of-view:

$$y = \frac{\sin\sigma_{\lim}}{\eta} > 1 \tag{12}$$

that is

$$\sin\sigma_{\lim} > \eta \tag{13}$$

It can be guaranteed that regardless of the desired line-of-sight angle, the final time target is always within the seeker's field-of-view. If the relationship does not meet Eq. (13) within the range $q_F \in (\theta_t - \pi, \theta_t + \pi)$, the desired line-of-sight angle must be within the limit range shown in Fig. 4. Otherwise, the target will exceed the field-of-view range at the final time.

In order to successfully intercept the target with the desired impact angle, the line-of-sight angle at the initial position should be correctly selected. Combined with the missile's maneuverability and considering the missile's flight stability requirements, the following two line-of-sight angle selection region types are defined: the extreme line-of-sight angle selection region and the ideal line-of-sight angle selection region.

Definition 2: From the perspective of the missile's maneuverability, we define the set

$$A = \{(q_{\min 0}, q_{\max 0}) | q(t) \in [q_{\min}(t), q_{\max}(t)] \text{ for } \forall t \in [t_0, t_f], r(t_f) < R_{miss}, |a_m(t)| \leq a_{m\max}\}$$

as the extreme line-of-sight angle selection region of the missile M at time t_0 during the flight, with an acceleration of no more than $a_{m\max}$ for target T. In this region, all line-of-sight angles that meet these conditions guarantee that the missile can theoretically intercept the target with maneuverability that does not exceed the maximum acceleration.

Definition 3: When the missile's acceleration is lower than the maximum acceleration, for the ideal missile interception scenario, we hope that during the stage where the missile approaches the target, the initial moment acceleration is the maximum acceleration of the entire flight process, i.e., $\forall t \in [t_0, t_f], a_m(t_0) \geq a_m(t)$. Thus, we call the collection

$$B = \{(q_{\min 0}, q_{\max 0}) | q(t) \in [q_{\min}(t), q_{\max}(t)], a_m(t) \leq a_m(t_0) \text{ for } \forall t \in [t_0, t_f], r(t_f) < R_{miss}\}$$

as the ideal line-of-sight angle selection region of missile M to the target T at time t_0. The definition of the ideal line-of-sight angle selection region indicates that when a missile wants to intercept a target in the extreme selection region but outside the ideal selection region, the acceleration command should exceed the current command value.

B. THE LINE-OF-SIGHT ANGLE SELECTION REGION OF THE IMPACT-ANGLE CONSTRAINT GUIDANCE LAW UNDER OPEN-LOOP CONDITIONS

From Eq. (5), we derive the missile's flight-path angle at the final time so that at the initial moment t_0, we can get the average rate of change of the flight-path angle in the $t_F - t_0$ time:

$$\bar{\dot{\theta}}_m = \frac{\theta_{mF} - \theta_{m0}}{t_F - t_0} \tag{14}$$

Since the change in the flight-path angle is related to the missile's speed and acceleration, by combining Eqs. (1) and (8), the flight-path angle rate of the initial moment t_0 is:

$$\dot{\theta}_m = N_1 \dot{q} + \frac{N_2(q - q_F)}{t_F - t_0} \tag{15}$$

Using the Cauchy inequality and giving for function $f(x)$ the maximum boundary $f_{\max}$ or the smallest boundary $f_{\min}$, we obtain:

$$x f_{\min} \leq \frac{x}{n} \sum_{i=1}^{n} f(\frac{ix}{n}) \leq x f_{\max} \tag{16}$$

where n is a positive integer.

By synthesizing Eqs. (14), (15), and (16), it is possible to obtain the extreme line-of-sight angle selection region at any time, meeting:

$$|(\theta_m - \theta_{mF}) \sin(q + \Phi_1)| \leq \frac{r a_{\max}}{V_m V_r} \tag{17}$$

where

$$\tan \Phi_1 = \frac{\eta \cos \theta_t - \cos \theta_m}{\eta \sin \theta_t - \sin \theta_m} \tag{18}$$

where Φ_1 is the auxiliary angle of the trigonometric function, with the corresponding proof presented in Appendix A.

The ideal line-of-sight angle selection region at any time satisfies the following:

$$\frac{V_m |\theta_{mf} - \theta_m|}{(n+2)V_r} \leq \left| -\frac{2\sin(q + \Phi_2)}{\sin(q + \Phi_1)} + (n+1)(q - q_F) \right| \tag{19}$$

where

$$\tan \Phi_2 = \frac{\eta \sin \theta_t - \sin \theta_m}{\cos \theta_m - \eta \cos \theta_t} = -\frac{1}{\tan \Phi_1} \tag{20}$$

where Φ_2 is the auxiliary angle of the trigonometric function, with the corresponding proof presented in Appendix B.

The relationship between the extreme and the ideal line-of-sight angle selection regions on missile acceleration is further elaborated: At the initial moment,

(A) If the extreme and the ideal line-of-sight angle selection regions coincide and the missile line-of-sight angle is on the selection region boundary, then in $t \in [t_0, t_f]$, the missile always flies with maximum acceleration.

(B) If the extreme and the ideal line-of-sight angle selection regions coincide, and the missile line-of-sight angle is in the selected region, then in $t \in [t_0, t_x]$, $t_x < t_f$ the missile flies with maximum acceleration, and in $t \in [t_x, t_f]$, $t_x < t_f$ the missile acceleration falls.

(C) If the extreme line-of-sight angle selection region is greater than the ideal line-of-sight angle selection region, and the missile line-of-sight angle is outside the ideal line-of-sight angle selection region within the extreme line-of-sight angle selection region, the missile acceleration is lower than the maximum acceleration but shows an upward trend.

(D) If the extreme line-of-sight angle selection region is greater than the ideal line-of-sight angle selection region, and the missile line-of-sight angle is within the ideal line-of-sight angle selection region, the missile acceleration is lower than the maximum acceleration and shows a downward trend.

(E) If the extreme line-of-sight angle selection region is greater than the ideal line-of-sight angle selection region and the missile line-of-sight angle is at the boundary of the ideal line-of-sight angle selection region, the missile acceleration is lower than the maximum acceleration, and the rate of change is zero.

(F) If the angle of sight of the missile is outside the extreme line-of-sight angle selection region, the missile cannot intercept the target with the desired impact angle under the currently rated acceleration.

When the target is fixed, [28] proposes an extended optimal impact-angle-control guidance law, simplifying Eq. (8) to:

$$a_{EOIACGL} = \frac{2(n+2)V_m(q-\theta_m)}{t_{go}} + \frac{(n+1)(n+2)V_m(q-q_F)}{t_{go}} \tag{21}$$

In this case, by combining Eqs. (3) and (21) we obtain the ideal line-of-sight angle selection region at any time to satisfy the:

$$\frac{|\theta_{mF}-\theta_m|}{n+2} \le |(n+3)q-(n+1)q_F-2\theta_m| \tag{22}$$

The ideal line-of-sight angle selection region at this point can be solved directly without requiring iterative calculations.

C. THE IMPACT ANGLE CONSTRAINT GUIDELINE OF THE LINE-OF-SIGHT ANGLE SELECTION REGION UNDER CLOSED-LOOP CONDITIONS

In [28], the authors provided a closed-loop solution involving acceleration instructions with an impact-angle constraint guidance law:

$$\frac{a_c(t)}{V_r q_F} = \frac{N_2(n+3)}{t_F-t_0}\left[\frac{t_F-t}{t_F-t_0}-\frac{n+1}{n+3}\right]\left(\frac{t_F-t}{t_F-t_0}\right)^n \tag{23}$$

At this point, the closed-loop interpretation of the ideal line-of-sight angle selection region can be elaborated as follows: for $t \in [t_0, t_f]$, the $a_c(t)$ represented by Eq. (23) should always be satisfied $|a_c(t)| \le a_{m\max}$. Unlike the ideal line-of-sight angle selection region calculation under the open loop condition, where the ideal line-of-sight angle selection region under the open loop condition meets the ideal line-of-sight angle selection region definition and the restriction conditions for the gradual guidance instruction reduction. The closed loop condition must only meet the definition conditions, with the requirement to meet the guidance instructions gradually decreasing. There-fore, the ideal line-of-sight angle selection region under the closed-loop condition of this section is not less than the ideal line-of-sight angle selection region sought under the open-loop condition.

Eq. (23) can be expressed as:

$$a_c(t) = -\frac{V_r q_F \dot{r}(n+1)(n+2)(n+3)}{r}\cdot\left[\frac{\dot{r}t}{r}+\frac{2}{n+3}\right]\left(1+\frac{\dot{r}t}{r}\right)^n \tag{24}$$

Eq. (24) is time-derived to obtain:

$$\frac{da_c(t)}{dt} = -\frac{V_r q_F \dot{r}^2(n+1)(n+2)(n+3)}{r^2}\cdot\left(\left(1+\frac{\dot{r}t}{r}\right)^n + n\left(1+\frac{\dot{r}t}{r}\right)^{n-1}\left[\frac{\dot{r}t}{r}+\frac{2}{n+3}\right]\right) \tag{25}$$

1) $n = 0$, I.E. $N_1 = 2(n+2) = 4$, $N_2 = (n+1)(n+2) = 2$,

$$\frac{da_c(t)}{dt} = -\frac{6V_r q_F \dot{r}^2}{r^2} \tag{26}$$

when $t \in [0, t_F)$, we obtain:

$$\begin{cases} t < -\dfrac{r}{\dot{r}} = t_F, \ \dfrac{da_c(t)}{dt} < 0 & q_F \in (0,\pi) \\ t < -\dfrac{r}{\dot{r}} = t_F, \ \dfrac{da_c(t)}{dt} > 0 & q_F \in (-\pi,0) \end{cases} \tag{27}$$

Therefore, the ideal line-of-sight angle selection region under the closed-loop condition of $n = 0$ should meet the following:

$$\begin{cases} |a_c(t_0)| \le a_{m\max} \\ |a_c(t_F)| \le a_{m\max} \end{cases} \tag{28}$$

Replace Eq. (28) with Eq. (24) under the closed-loop condition so that the ideal line-of-sight angle selection region meets the following:

$$\begin{cases} |-q_F \sin(q+\Phi_1)| \le \dfrac{r a_{m\max}}{4V_r^2} & t = 0 \\ |-q_F \sin(q+\Phi_1)| \le \dfrac{r a_{m\max}}{2V_r^2} & t = t_F \end{cases} \tag{29}$$

2) $n = 1$, I.E., $N_1 = 2(n+2) = 6$, $N_2 = (n+1)(n+2) = 6$.

$$\frac{da_c(t)}{dt} = -\frac{24V_r q_F \dot{r}^2}{r^2}\left(\frac{3}{2}+\frac{2\dot{r}t}{r}\right) \tag{30}$$

when $t \in [0, t_F)$, we obtain:

$$\frac{da_c(t)}{dt} = -\frac{24V_r q_F \dot{r}^2}{r^2}\left(\frac{3}{2}+\frac{2\dot{r}t}{r}\right) \tag{31}$$

Therefore, the ideal line-of-sight angle selection region under the closed-loop condition of $n = 1$ should meet the following:

$$\begin{cases} |a_c(t_0)| \le a_{m\max} \\ \left|a_c(\dfrac{3t_F}{4})\right| \le a_{m\max} \\ |a_c(t_F)| \le a_{m\max} \end{cases} \tag{32}$$

Replace Eq. (33) with Eq. (24) under the closed-loop condition so that the ideal line-of-sight angle selection region meets the following:

$$\begin{cases} |-q_F \sin(q+\Phi_1)| \le \dfrac{r a_{m\max}}{12V_r^2} & t = 0 \\ |q_F \sin(q+\Phi_1)| \le \dfrac{2r a_{m\max}}{3V_r^2} & t = \dfrac{3}{4}t_F \end{cases} \tag{33}$$

D. CHARACTERISTIC ANALYSIS OF THE EXTREME SELECTION REGION AND THE IDEAL SELECTION REGION

From the extreme selection region definition, it can be seen that the acceleration limit of the extreme selection region is the missile's allowable acceleration. Thus, combining Eqs. (5), (19), and (20) force the set of the t_0 extreme selection region on the line-of-sight q to meet:

$$|\sin(q+\Phi_1)| \le \frac{r a_{\max}}{V_m V_r |(\theta_{m0}-\theta_{mF})|} \tag{34}$$

So when:

$$r \ge \frac{V_m V_r |(\theta_{m0}-\theta_{mF})|}{a_{\max}} \tag{35}$$

the missile has an omnidirectional attack and can be expected to intercept the target at this distance range by capturing the target. According to Eq. (35), during the missile flight, the closer the flight-path angle of the missile to the missile terminal flight-path angle θ_{mF} under the constraint of the impact angle, the smaller the corresponding permissible distance when the missile is omnidirectional.

Next, the ideal line-of-sight angle selection region of Eq. (19) is analyzed. Let:

$$f(q) = -\frac{2\sin(q+\Phi_2)}{\sin(q+\Phi_1)} + (n+1)(q-q_F) \tag{36}$$

For $\tan\Phi_1 \tan\Phi_2 = -1$, i.e., $\Phi_1 = \Phi_2 \pm \frac{\pi}{2}$, Eq. (36) can be changed as:

$$\begin{aligned} f(q) &= -\frac{2\sin(q+\Phi_2)}{\sin(q+\Phi_2 \pm \frac{\pi}{2})} + (n+1)(q-q_F) \\ &= \mp 2\tan(q+\Phi_2) + (n+1)(q-q_F) \end{aligned} \tag{37}$$

Specifying Eq. (37) allows for a derivative analysis of:

$$\frac{df(q)}{dq} = \frac{\mp 2}{\cos^2(q+\Phi_2)} + (n+1) \tag{38}$$

Also $\frac{1}{\cos^2(q+\Phi_2)} \geq 1$, so in the case of $n = 0$ or $n = 1$, the plus or minus of $\frac{df(q)}{dq}$ is related to the size of Φ_1 and Φ_2, namely:

$$\begin{cases} \dfrac{df(q)}{dq} \leq 0 \ \Phi_1 = \Phi_2 + \dfrac{\pi}{2} \\ \dfrac{df(q)}{dq} \geq 0 \ \Phi_1 = \Phi_2 - \dfrac{\pi}{2} \end{cases} \tag{39}$$

From Eq. (39), the function $f(q)$ is monotonic, and to make the line-of-sight angle have a solution on $q \in [\theta_m - \sigma_{\lim}, \theta_m + \sigma_{\lim}]$, the following must hold:

$$\min\{|f(\theta_m + \sigma_{\lim})|, |f(\theta_m - \sigma_{\lim})|\} \geq \frac{|\theta_{mf} - \theta_{m0}| V_m}{(n+2)V_r} \tag{40}$$

By combining Eqs. (5) and (20), Eq. (40) may be further expressed as (41), shown at the bottom of the page.

When the flight-path angle of the missile satisfies the relationship described in Eq. (41), the ideal line-of-sight angle selection region envelops the entire seeker viewing angle range.

Through the analysis of the line-of-sight angle selection region of Eqs. (29) and (33) under closed loop conditions, the time when the most restriction on the line-of-sight angle selection region is the initial time. So the line-of-sight angle selection region un-der closed-loop conditions can be written as:

$$\begin{cases} |-q_F \sin(q+\Phi_1)| \leq \dfrac{ra_{m\max}}{4V_r^2} & n = 0 \\ |-q_F \sin(q+\Phi_1)| \leq \dfrac{ra_{m\max}}{12V_r^2} & n = 1 \end{cases} \tag{42}$$

The next section of the Numerical Simulation compares the line-of-sight angle se-lection region under open-loop and closed-loop conditions.

TABLE 1. Simulation parameters.

SCENARIO	Initial distance	Missile speed	Target speed	The initial flight-path angle of the missile	The initial flight-path angle of the target	Impact angle constraint
Air-to-air missiles against interception	15000m/8000m	1200m/s	500m/s	10deg (head-on) -10deg (tail-chase)	-170deg (head-on) 10deg(tail-chase)	-10deg
Air-to-ground strikes	4000m	400m/s	100m/s	0	-180deg	-60deg, -90deg

IV. NUMERICAL SIMULATION

This section simulates different combat scenarios, which analyze the effects of acceleration and investigate how the initial line-of-sight angle and the impact angle constraint will determine the line-of-sight angle selection region for the two situations of head-on interception and tail-chase attack. Additionally, the simulation results of the selection region consider different conditions. Let the navigation factor be $n = 1$, and the remaining relevant simulation parameters are reported in Table 1.

A. AIR-TO-AIR MISSILES AGAINST INTERCEPTION

1) HEAD-ON

The initial line-of-sight angle must be $q_0 = 20°$ and let the missile acceleration limit be 35g, 40g, and 45g, according to the simulation parameters in Table 1. When the missile successfully hits the target, $\theta_{mF} = -18.2°$, the corresponding simulation results are illustrated in Figure 5.

Fig. 5 highlights that different acceleration limits correspond to different extreme line-of-sight angle selection regions under the same conditions. Additionally, the missile's

$$\begin{cases} \left|\dfrac{(n+1)(\theta_m + \sigma_{\lim} - q_F) - 2\tan(\theta_m + \sigma_{\lim} + \arctan\frac{\eta\sin\theta_t - \sin\theta_m}{\cos\theta_m - \eta\cos\theta_t})}{q_F + \arcsin(\eta\sin(\theta_t - q_F)) - \theta_m}\right| \geq \dfrac{V_m}{(n+2)V_r}, & \Phi_1 = \Phi_2 + \dfrac{\pi}{2} \\ \left|\dfrac{(n+1)(\theta_m - \sigma_{\lim} - q_F) + 2\tan(\theta_m - \sigma_{\lim} + \arctan\frac{\eta\sin\theta_t - \sin\theta_m}{\cos\theta_m - \eta\cos\theta_t})}{q_F + \arcsin(\eta\sin(\theta_t - q_F)) - \theta_m}\right| \geq \dfrac{V_m}{(n+2)V_r}, & \Phi_1 = \Phi_2 - \dfrac{\pi}{2} \end{cases} \tag{41}$$

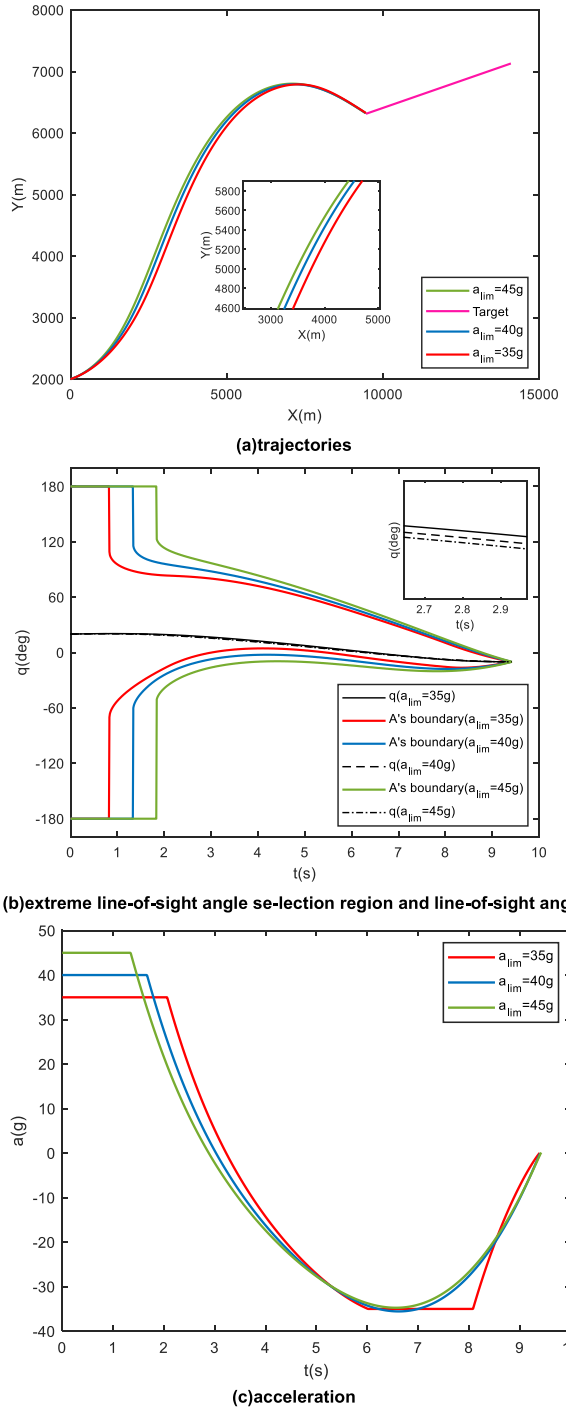

FIGURE 5. Simulation results of the extreme line-of-sight angle selection region (head-on).

extreme line-of-sight angle selection region increases with the increase of acceleration limit during flight, while different acceleration limit will impose a different missile trajectory. However, as long as the missile can finally hit the target, the missile's line-of-sight angle is always within the extreme line-of-sight angle selection region.

The initial line-of-sight angle is $q_0 = 20°, 0°, -20°$, and the acceleration limit of the missile is 35g. The corresponding simulation results are depicted in Fig. 6.

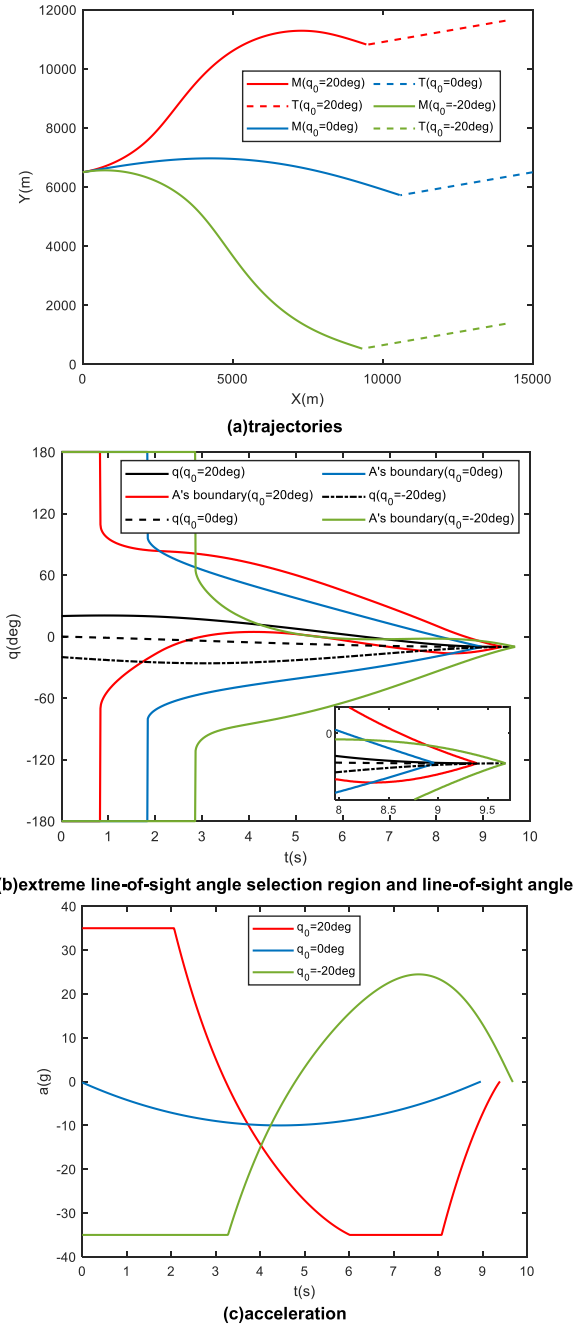

FIGURE 6. Simulation results of the extreme line-of-sight angle selection region (head-on).

Fig. 6 reveals that under the same conditions, a different initial line-of-sight angle corresponds to different extreme line-of-sight angle selection regions, and the range of selected regions is related to the line-of-sight angle.

2) TAIL-CHASE

The initial line-of-sight angle must be $q_0 = 20°$ and let the missile acceleration limit be 35g, 40g, and 45g, according to the simulation parameters presented in Table 1. When the missile successfully hits the target, $\theta_{mF} = -1.8°$, the corresponding simulation result is illustrated in Figure 7.

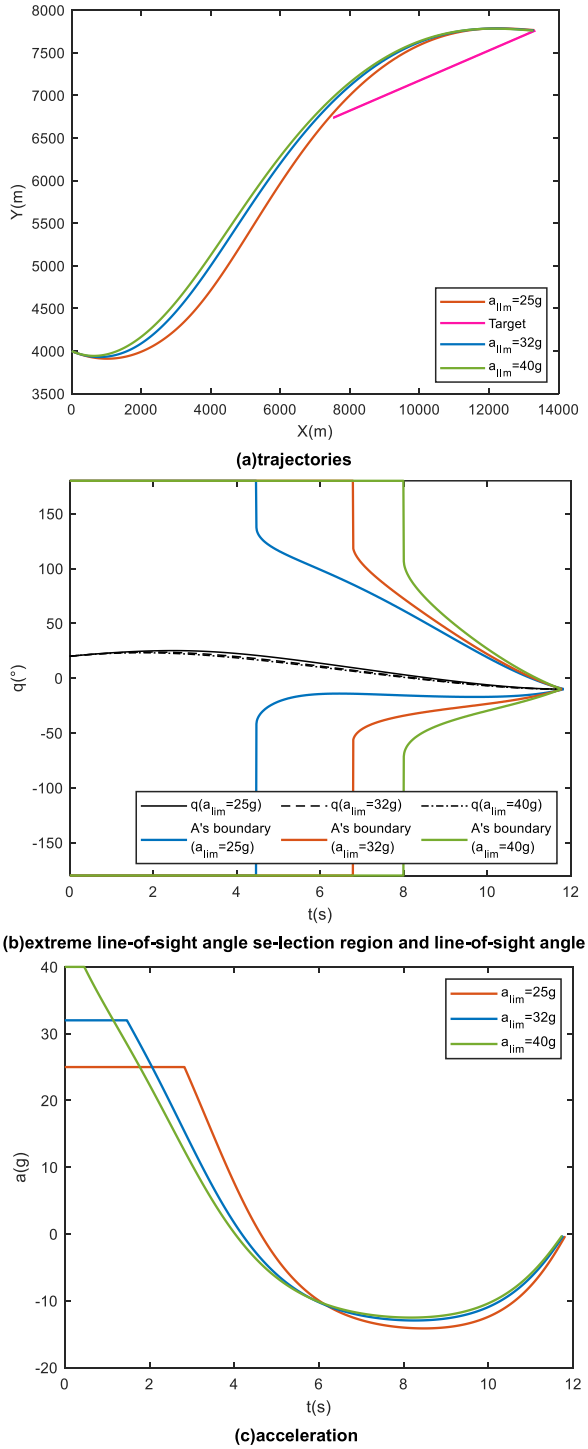

FIGURE 7. Simulation results of the extreme line-of-sight angle selection region (tail-chase).

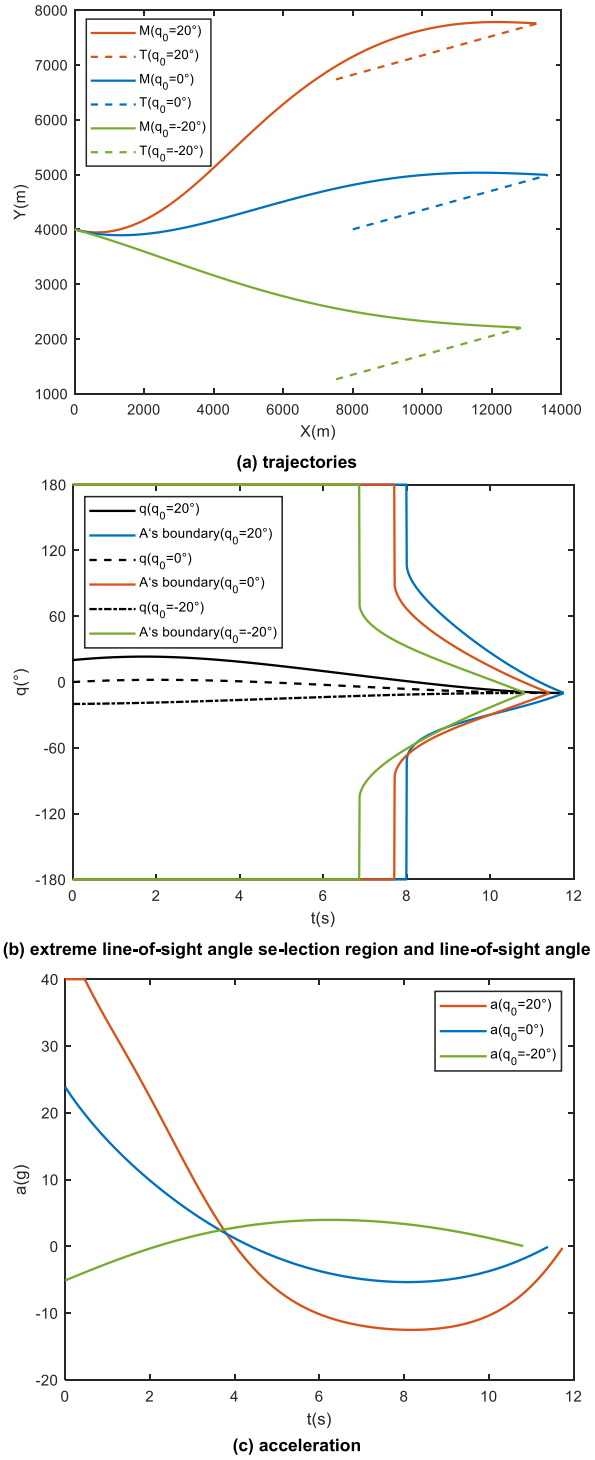

FIGURE 8. Simulation results of the extreme line-of-sight angle selection region (tail-chase).

Fig. 7 infers that in a tail-chase attack, the nature of the extreme line-of-sight angle selection region due to acceleration restrictions is the same as that of head-on interception. However, the maximum acceleration required to achieve the same effect as a head-on interception is small, i.e., under the same conditions, the tail-chasing attack is larger than the line-of-sight angle selection region of the head-on interception.

Let the initial line-of-sight angle be $q_0 = 20°, 0°, -20°$, and the acceleration limit of the missile is 40g. The simulation results are presented in Fig. 8.

Fig. 8 highlights that under the tail-chase attack condition, the extreme line-of-sight angle selection region exhibits the same nature as the head-on interception due to the difference in the initial line-of-sight angle.

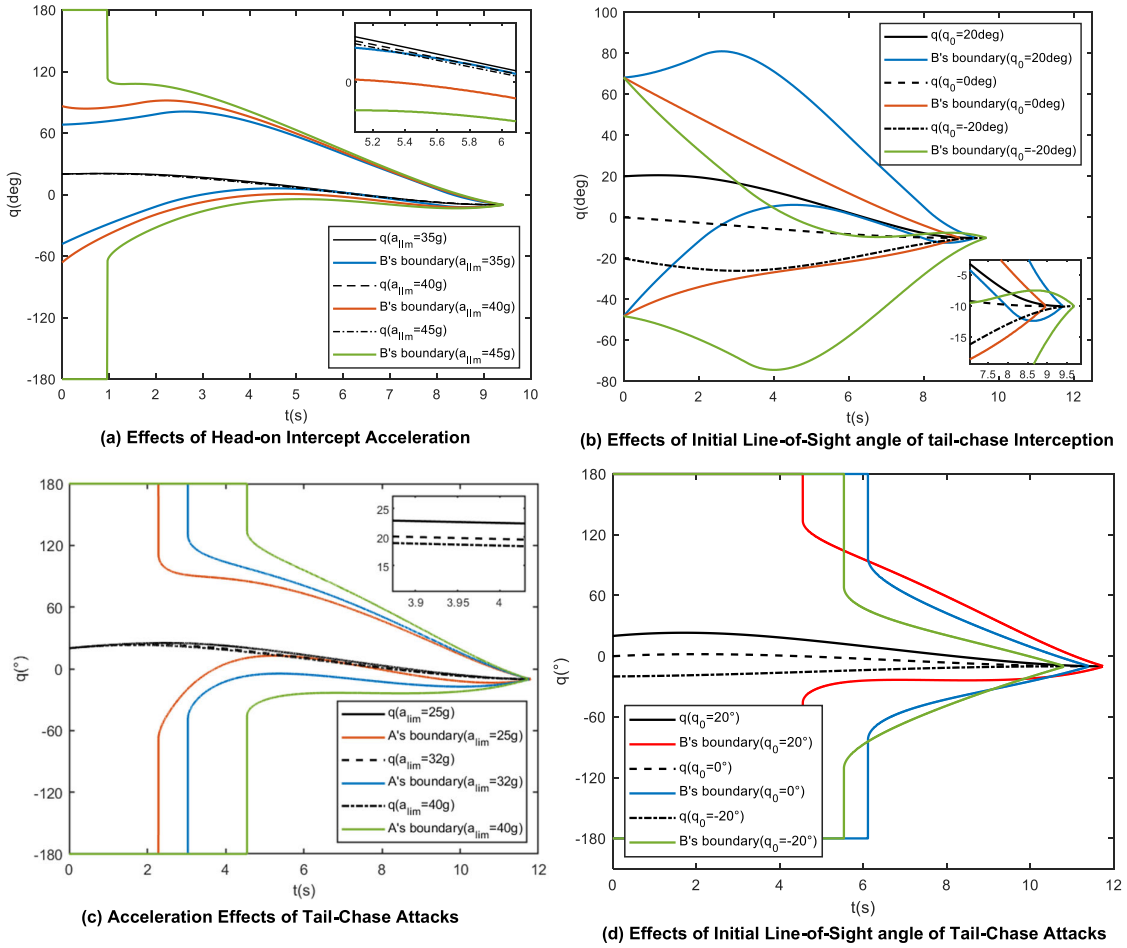

FIGURE 9. Simulation results of the ideal line-of-sight angle selection region.

3) IDEAL LINE-OF-SIGHT ANGLE SELECTION REGION SIMULATION

The ideal line-of-sight angle selection region is the same as the simulation conditions of the head-on interception and the tail-chase attack in the extreme line-of-sight angle selection region. Hence, the initial line-of-sight is $q_0 = 20°$, and the missile acceleration limit is 35g, 40g, and 45g, respectively. The initial line-of-sight angle is $q_0 = 20°, 0°, -20°$, and the missile's acceleration limit is 25g, 32g, and 40g, respectively. The initial line-of-sight and the missile acceleration limits are 25g, 32g, and 40g, respectively, the initial angle of sight is $q_0 = 20°, 0°, -20°$, and the acceleration limit of the missile is 40g. The simulation results are illustrated in Fig. 9.

Fig. 9 reveals that the properties exhibited by the ideal line-of-sight angle selection region and the extreme line-of-sight angle selection region are the same considering acceleration limit, initial line-of-sight angle, and attack mode.

Fig. 10 compares the results presented in Figs. 5 to 9, highlighting that the ideal line-of-sight angle selection region is always less than the extreme line-of-sight angle selection region. Fig. 10 (a) can be obtained when the acceleration limit is larger, and the ideal line-of-sight angle selection region is closer to the extreme line-of-sight angle selection region. Thus, the greater the acceleration, the greater the impact on the line-of-sight angle selection region than the guidance law on the line-of-sight angle se-lection region.

Comprehensive analysis of Figures 5 to 4, we can find that in the process of the missile hitting the target, the line-of-sight selection region also gradually shrinks and tends to the established end state, but the missile's line-of-sight angle always falls in the selection region, so when the line-of-sight angle is in the selection region, the probability of the missile hitting the target is higher than that outside the line-of-sight selection region.

B. AIR-TO-GROUND STRIKES

To observe the influence of the terminal angle restriction on the line-of-sight angle selection region, let the desired impact angles be $q_F = -90°$ and $q_F = -60°$, and the $\theta_{mF} = -104.5°$ and $\theta_{mF} = -72.5°$, respectively. The simulation results are presented in Fig. 11.

Fig. 11 demonstrates that when the impact angle constraint is restricted, the line-of-sight angle selection region becomes narrower, that is, the line-of-sight angle selection region becomes narrower when the missile must turn over a larger angle of sight angle to achieve the constraint condition of the impact angle.

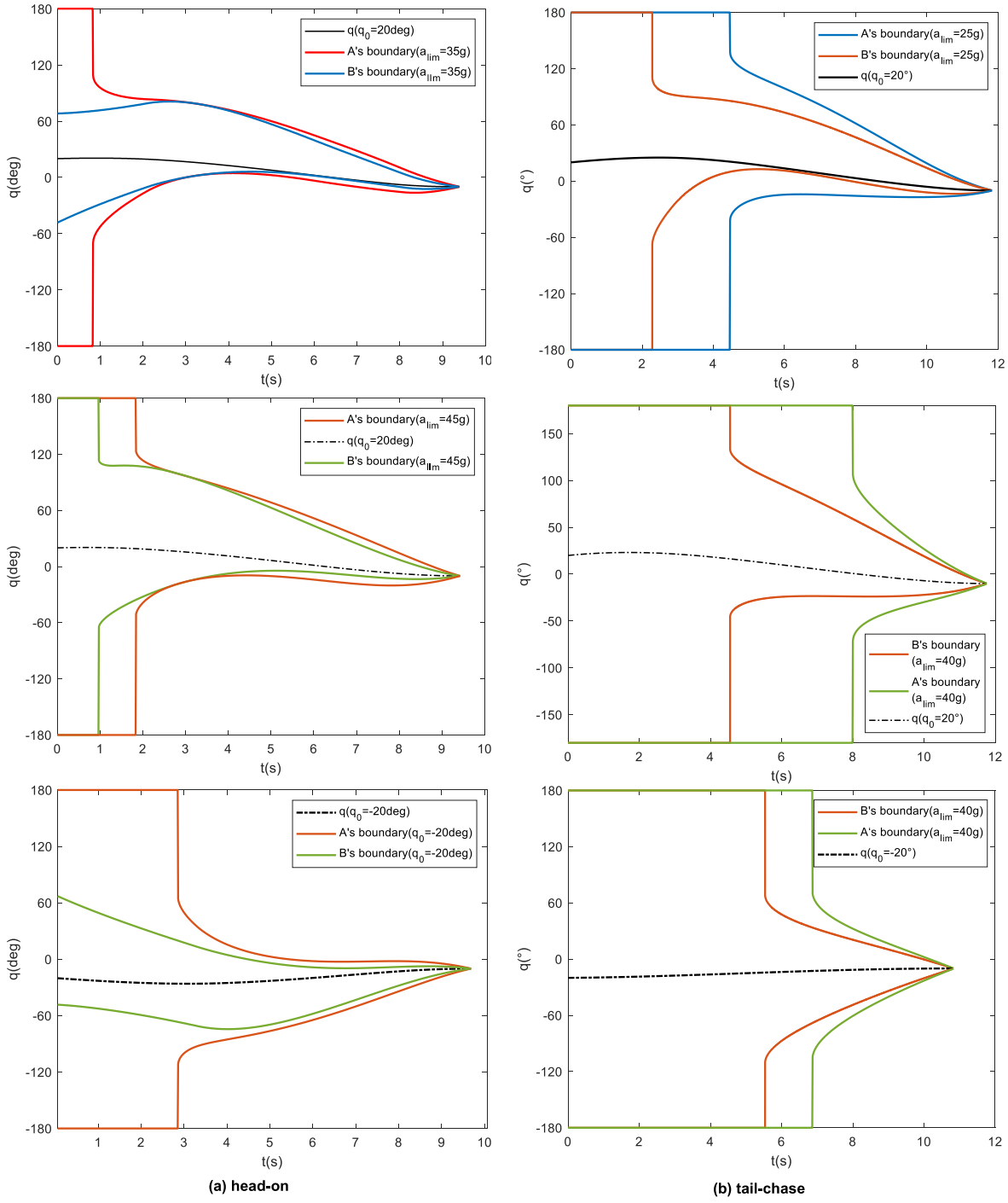

FIGURE 10. Simulation results of the extreme line-of-sight angle selection region.

V. CONCLUSION

This paper studies the line-of-sight angle selection region for intercepting high-speed non-maneuvering targets with impact angle constraints, combined with the missile field-of-view limit, the given relationship between the terminal missile line-of-sight angle and the flight-path angle, and the derived selection set expression of the line-of-sight angle restriction at the end of the missile's trajectory. Combined with the closed-loop solution of the Cauchy-Schwartz inequality and the acceleration command of the guidance law, the mathematical expression of the extreme line-of-sight angle selection region and the ideal line-of-sight angle selection region of the impact-angle constraint guidance law intercepting high-speed non-maneuvering targets is derived. Moreover, characteristic analysis and simulation studies are con-ducted. The simulation results demonstrate that during the missile's flight hitting the target with the desired impact angle, the line-of-sight angle always falls within the extreme line-of-sight

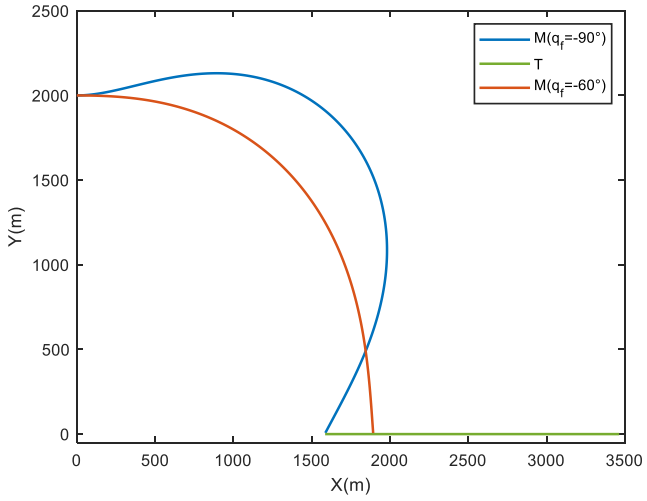

(a) Trajectories

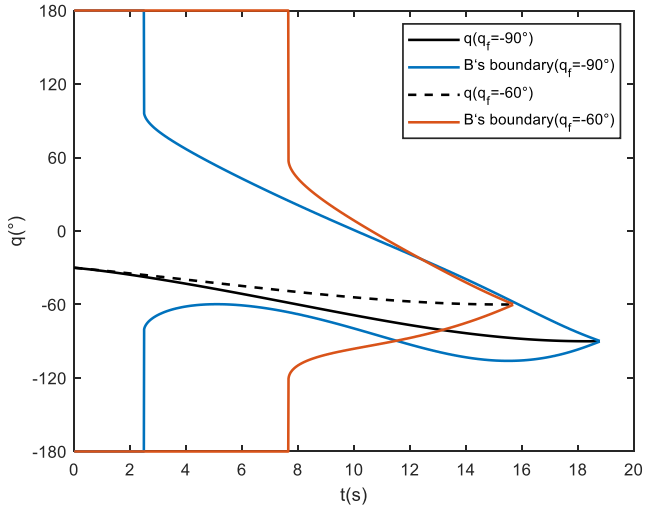

(b) line-of-sight angle selection region

FIGURE 11. Comparison of simulation results of the extreme line-of-sight angle selection region and the ideal line-of-sight angle selection region.

angle selection region. Additionally, the results highlight that the tail-chase attack has a larger range of line-of-sight angle selection region than the head-on interception, and the selection region's range increases with the acceleration limit.

Considering the flexibility and complexity of the engagement scene, the interception capability of the missile can be improved by adjusting the position and the direction of relative velocity at the beginning of the guidance process. As follow-up research, the line-of-sight angle selection region in the three-dimensional space or for maneuvering targets should be investigated.

APPENDIX A
DERIVATION OF THE IDEAL LINE-OF-SIGHT ANGLE SELECTION REGION

Obtained by Eq. (16):

$$\left|\frac{\theta_{mf}-\theta_{m0}}{t_{go}}\right| \le \frac{a_{\max}}{V_m} \tag{43}$$

where $t_{go} = -r/\dot{r} = \frac{-r}{\dot{r}}$ and $\dot{r} = V_t\cos(\theta_t - q) - V_m\cos(q-\theta_m)$. Eq. (43) can be changed as:

$$\left|\frac{\theta_{mf}-\theta_{m0}}{-r}\left(V_t\cos(\theta_t-q) - V_m\cos(q-\theta_m)\right)\right| \le \frac{a_{\max}}{V_m} \tag{44}$$

Eq. (44) can be rewritten as:

$$\frac{ra_{\max}}{V_m} \ge |(\theta_{m0}-\theta_{mF})\cdot((V_t\sin\theta_t - V_m\sin\theta_m)\sin q + (V_t\cos\theta_t - V_m\cos\theta_m)\cos q)| \tag{45}$$

Using the auxiliary angle formula, Eq. (45) can be arranged as follows:

$$\left|(\theta_{m0}-\theta_{mF})\cdot\left(\sqrt{V_t^2+V_m^2-2V_tV_m\cos(\theta_m-\theta_t)}\sin(q+\Phi_1)\right)\right| \le \frac{ra_{\max}}{V_m} \tag{46}$$

where

$$\tan\Phi_1 = \frac{V_t\cos\theta_t - V_m\cos\theta_m}{V_t\sin\theta_t - V_m\sin\theta_m} = \frac{\eta\cos\theta_t - \cos\theta_m}{\eta\sin\theta_t - \sin\theta_m} \tag{47}$$

Therefore Eq. (46) can be rewritten as:

$$|(\theta_{m0}-\theta_{mF})\sin(q+\Phi_1)| \le \frac{ra_{\max}}{V_m\sqrt{V_t^2+V_m^2-2V_tV_m\cos(\theta_m-\theta_t)}} \tag{48}$$

i.e.:

$$|(\theta_{m0}-\theta_{mF})\sin(q+\Phi_1)| \le \frac{ra_{\max}}{V_mV_r} \tag{49}$$

APPENDIX B
DERIVATION OF THE EXTREME LINE-OF-SIGHT ANGLE SELECTION REGION

Obtained by Eq. (16):

$$\left|\frac{\theta_{mf}-\theta_{m0}}{t_{go}}\right| \le \left|\frac{a_m}{V_m}\right| \tag{50}$$

and

$$a_m = 2(n+2)V_r\dot{q} + \frac{(n+1)(n+2)V_r(q-q_F)}{t_{go}} \tag{51}$$

Combined with the missile nonlinear engagement kinematics, Eq. (51) is rewritten as:

$$|\theta_{mf}-\theta_{m0}| \le |\frac{-2(n+2)V_r\dot{q}r}{\dot{r}V_m} + \frac{(n+1)(n+2)V_r(q-q_F)}{V_m}| \tag{52}$$

therefore

$$|\theta_{mf}-\theta_{m0}|\frac{V_m}{(n+2)V_r} \le |(n+1)(q-q_F) - \frac{2(\eta\sin(\theta_t-q)+\sin(q-\theta_m))}{\eta\cos(\theta_t-q)-\cos(q-\theta_m)}| \tag{53}$$

Eq. (53) can be expressed as (54), shown at the top of the next page, meanwhile (55), as shown at the top of the next page.

$$\left|\theta_{mf}-\theta_{m0}\right|\frac{V_m}{(n+2)V_r}\le\left|(n+1)(q-q_F)-2\frac{\eta\sin\theta_t\cos q-\eta\cos\theta_t\sin q+\sin q\cos\theta_m-\cos q\sin\theta_m}{\eta\cos\theta_t\cos q+\eta\sin\theta_t\sin q-\cos q\cos\theta_m-\sin q\sin\theta_m}\right| \tag{54}$$

$$\left|\theta_{mf}-\theta_{m0}\right|\frac{V_m}{(n+2)V_r}\le\left|(n+1)(q-q_F)-2\frac{(\cos\theta_m-\eta\cos\theta_t)\sin q+(\eta\sin\theta_t-\sin\theta_m)\cos q}{(\eta\sin\theta_t-\sin\theta_m)\sin q+(\eta\cos\theta_t-\cos\theta_m)\cos q}\right| \tag{55}$$

By using the auxiliary angle formula, Eq. (55) is changed to:

$$\begin{aligned}&\frac{V_m\left|\theta_{mf}-\theta_{m0}\right|}{(n+2)V_r}\\&\le\left|(n+1)(q-q_F)-\frac{\sin(q+\Phi_2)}{\sin(q+\Phi_3)}\right.\\&\qquad\left.\cdot\frac{2\sqrt{(\cos\theta_m-\eta\cos\theta_t)^2+(\eta\sin\theta_t-\sin\theta_m)^2}}{\sqrt{(\eta\sin\theta_t-\sin\theta_m)^2+(\eta\cos\theta_t-\cos\theta_m)^2}}\right|\end{aligned} \tag{56}$$

where

$$\begin{aligned}\tan\Phi_2&=\frac{\eta\sin\theta_t-\sin\theta_m}{\cos\theta_m-\eta\cos\theta_t}=-\frac{1}{\tan\Phi_1}\\\tan\Phi_3&=\frac{\eta\cos\theta_t-\cos\theta_m}{\eta\sin\theta_t-\sin\theta_m}=\tan\Phi_1\end{aligned} \tag{57}$$

The final result is:

$$\frac{V_m\left|\theta_{mf}-\theta_{m0}\right|}{(n+2)V_r}\le\left|-\frac{2\sin(q+\Phi_2)}{\sin(q+\Phi_1)}+(n+1)(q-q_F)\right| \tag{58}$$

REFERENCES

[1] P. Zarchan, *Tactical and Strategic Missile Guidance*. Reston, VA, USA: American Institute of Aeronautics and Astronautics, 2019.
[2] N. K. Singh and S. Hota, "Moving target interception guidance law for any impact angle with field-of-view constraint," in *Proc. AIAA Scitech Forum.*, 2021, p. 1462.
[3] H.-G. Kim, J.-Y. Lee, H. J. Kim, H.-H. Kwon, and J.-S. Park, "Look-angle-shaping guidance law for impact angle and time control with field-of-view constraint," *IEEE Trans. Aerosp. Electron. Syst.*, vol. 56, no. 2, pp. 1602–1612, Apr. 2020.
[4] Y. R. Sharma and A. Ratnoo, "A bearings-only trajectory shaping guidance law with look-angle constraint," *IEEE Trans. Aerosp. Electron. Syst.*, vol. 55, no. 6, pp. 3303–3315, Dec. 2019.
[5] A. Ranjan, S. Hota, and N. K. Singh, "Three-stage proportional navigation for intercepting stationary targets with impact angle constraints," in *Proc. 6th Indian Control Conf. (ICC)*, Dec. 2019, pp. 379–384.
[6] J.-H. Kim, S.-S. Park, K.-K. Park, and C.-K. Ryoo, "Quaternion based three-dimensional impact angle control guidance law," *IEEE Trans. Aerosp. Electron. Syst.*, vol. 57, no. 4, pp. 2311–2323, Aug. 2021.
[7] D. Lee and H.-L. Choi, "Three-dimensional impact angle guidance laws for precision guided munition," in *Proc. IEEE Aerosp. Conf.*, Mar. 2019, pp. 1–8.
[8] R. Duvvuru, A. Maity, and J. Umakant, "Three-dimensional field of view and impact angle constrained guidance with terminal speed maximization," *Aerosp. Sci. Technol.*, vol. 126, Jul. 2022, Art. no. 107552.
[9] Y.-W. Kim, M.-G. Seo, and C.-H. Lee, "Investigation on energy-effective guidance-to-collision strategies for exo-atmospheric interceptors," *Aerosp. Sci. Technol.*, vol. 124, May 2022, Art. no. 107563.
[10] T. Han, Q. Hu, and M. Xin, "Three-dimensional approach angle guidance under varying velocity and field-of-view limit without using line-of-sight rate," *IEEE Trans. Syst., Man, Cybern. Syst.*, vol. 52, no. 11, pp. 7148–7159, Nov. 2022.
[11] K. S. Erer and R. Tekin, "Three-dimensional impact-angle control with biased proportional navigation," in *Proc. 30th Medit. Conf. Control Autom. (MED)*, Jun. 2022, pp. 409–413.
[12] W. Dong, C. Wang, J. Wang, and M. Xin, "Three-dimensional nonsingular cooperative guidance law with different field-of-view constraints," *J. Guid., Control, Dyn.*, vol. 44, no. 11, pp. 2001–2015, Nov. 2021.
[13] Y. Wang, H. Wang, D. Lin, and W. Wang, "Nonlinear guidance laws for maneuvering target interception with virtual look angle constraint," *IEEE Trans. Aerosp. Electron. Syst.*, vol. 58, no. 4, pp. 2807–2822, Aug. 2022.
[14] S. J. Yang, Q. Xia, and G. Q. Zhou, "Guidance strategy considering strapdown seeker minimum field-of-view angle constraint," *Acta Aeronautica et Astronautica Sinica*, vol. 41, no. S2, 2020, Art. no. 724449, doi: 10.7527/S1000-6893.2020.24449.
[15] Y. Chen, J. Wang, C. Wang, J. Shan, and M. Xin, "Three-dimensional cooperative homing guidance law with field-of-view constraint," *J. Guid., Control, Dyn.*, vol. 43, no. 2, pp. 389–397, Feb. 2020.
[16] L.-G. Lin and M. Xin, "Impact angle guidance using state-dependent (differential) Riccati equation: Unified applicability analysis," *J. Guid., Control, Dyn.*, vol. 43, no. 11, pp. 2175–2182, Nov. 2020.
[17] R. V. Nanavati, S. R. Kumar, and A. Maity, "Lead-angle-based three-dimensional guidance for angle-constrained interception," *J. Guid., Control, Dyn.*, vol. 44, no. 1, pp. 190–199, 2020.
[18] N. Cho and S. Lee, "Look-angle-constrained control of arrival time with exact knowledge of time-to-go," *J. Guid., Control, Dyn.*, vol. 44, no. 10, pp. 1902–1908, Oct. 2021.
[19] D. Mukherjee and S. R. Kumar, "Field-of-view constrained impact time guidance against stationary targets," *IEEE Trans. Aerosp. Electron. Syst.*, vol. 57, no. 5, pp. 3296–3306, Oct. 2021.
[20] D. Yu, H. Wang, J. Zhou, and K. Li, "Capturability analysis of TPN guidance law for circular orbital pursuit-evasion," *Trans. Jpn. Soc. Aeronaut. Space Sci.*, vol. 60, no. 6, pp. 347–354, 2017.
[21] L. Sun, P. Lian, and X. Chang, "Capturability of retro-augmented proportional navigation guidance law against higher speed maneuvering target," in *Proc. 21st AIAA Int. Space Planes Hypersonics Technol. Conf.*, Mar. 2017, p. 2203.
[22] K.-B. Li, H.-S. Shin, A. Tsourdos, and M.-J. Tahk, "Capturability of 3D PPN against lower-speed maneuvering target for homing phase," *IEEE Trans. Aerosp. Electron. Syst.*, vol. 56, no. 1, pp. 711–722, Feb. 2020.
[23] Z. Bai, K. Li, W. Su, and L. Chen, "Capture region of RTPN guidance law against arbitrarily maneuvering targets," *Acta Aeronautica et Astronautica Sinica*, vol. 41, no. 8, 2020, Art. no. 323947, doi: 10.7527/S1000-6893.2020.23947.
[24] S. Lee, S. Ann, N. Cho, and Y. Kim, "Capturability of guidance laws for interception of nonmaneuvering target with field-of-view limit," *J. Guid., Control, Dyn.*, vol. 42, no. 4, pp. 869–884, Apr. 2019.
[25] D. Mukherjee and D. Ghose, "Target capturability using agents in cyclic pursuit," *J. Guid., Control, Dyn.*, vol. 39, no. 5, pp. 1034–1045, May 2016.
[26] S. Ghosh, D. Ghose, and S. Raha, "Capturability of augmented pure proportional navigation guidance against time-varying target maneuvers," *J. Guid., Control, Dyn.*, vol. 37, no. 5, pp. 1446–1461, Sep. 2014.
[27] T. Han, Q. Hu, and M. Xin, "Analytical solution of field-of-view limited guidance with constrained impact and capturability analysis," *Aerosp. Sci. Technol.*, vol. 97, Feb. 2020, Art. no. 105586.
[28] H. Wang, D. Lin, Z. Cheng, and J. Wang, "Optimal guidance of extended trajectory shaping," *Chin. J. Aeronaut.*, vol. 27, no. 5, pp. 1259–1272, Oct. 2014.

[29] D. Cho and S.-H. Kim, "Direct impact angle control guidance for passive homing missiles," *Proc. Inst. Mech. Eng., G, J. Aerosp. Eng.*, vol. 234, no. 15, pp. 2139–2152, Dec. 2020.
[30] B. Kada, U. Ansari, and A. H. Bajodah, "Highly maneuvering target interception via robust generalized dynamic inversion homing guidance and control," *Aerosp. Sci. Technol.*, vol. 99, Apr. 2020, Art. no. 105749.
[31] N. Wang, X. Wang, N. Cui, Y. Li, and B. Liu, "Deep reinforcement learning-based impact time control guidance law with constraints on the field-of-view," *Aerosp. Sci. Technol.*, vol. 128, Sep. 2022, Art. no. 107765.
[32] A. Rizzi and J. M. Luckring, "Historical development and use of CFD for separated flow simulations relevant to military aircraft," *Aerosp. Sci. Technol.*, vol. 117, Oct. 2021, Art. no. 106940.
[33] R. de Celis, P. S. López, and L. Cadarso, "Sensor hybridization using neural networks for rocket terminal guidance," *Aerosp. Sci. Technol.*, vol. 111, Apr. 2021, Art. no. 106527.
[34] M. Ghoreyshi, A. Jirasek, P. Aref, and J. Seidel, "Computational aerodynamic investigation of long strake-tail missile configurations," *Aerosp. Sci. Technol.*, vol. 127, Aug. 2022, Art. no. 107704.
[35] E. H. Ata, T. Kaya, R. Tekin, and K. S. Erer, "Analysis of 2D impact angle control laws in 3D kinematics," in *Proc. 30th Medit. Conf. Control Autom. (MED)*, Jun. 2022, pp. 420–425.
[36] S. R. Kumar and D. Mukherjee, "Closed-form nonlinear impact angle guidance using state-dependent Riccati equation approach," in *Proc. Amer. Control Conf. (ACC)*, Jun. 2022, pp. 4017–4022.
[37] J. Wang, X. Ding, Y. Chen, C. Wang, and M. Xin, "Field-of-view constrained three-dimensional impact angle control guidance for speed-varying missiles," *IEEE Trans. Aerosp. Electron. Syst.*, vol. 58, no. 5, pp. 3992–4003, Oct. 2022.
[38] D.-Y. Lee, Y.-W. Kim, C.-H. Lee, and M.-J. Tahk, "Impact angle control guidance laws using finite-time-convergence control methods," in *Proc. 29th Medit. Conf. Control Autom. (MED)*, Jun. 2021, pp. 997–1002.
[39] X. S. Bui, D. H. Pham, V. G. Do, and V. B. Vo, "Analysing the sensitivity of the all-ways action mechanism upon impact on target," in *Proc. Int. Conf. Mil. Technol. (ICMT)*, Jun. 2021, pp. 1–5.

XIN SUN was born in Binzhou, Shandong, in 1998. She received the B.S. degree from the Nanjing University of Science and Technology, in 2020. She is currently pursuing the degree with the School of Aerospace Engineering, Beijing Institute of Technology.

Her main research interests include flight vehicle dynamics, guidance, and control.

HUI WANG was born in 1984. He received the Ph.D. degree in aerospace engineering from the Beijing Institute of Technology, Beijing, China, in 2012.

From 2012 to 2014, he was a Postdoctoral Researcher with the UAV Guidance and Control Team, Beihang University. He is currently a Lecturer with the School of Aerospace and Engineering, Beijing Institute of Technology. His research interests include advanced guidance and control technology.

KAIYANG GUO was born in Zhangjiakou, Hebei, in 1996. He received the M.A.Sc. degree in aeronautical and astronautical science and technology from the Beijing Institute of Technology, Beijing, China, in 2022.

He is currently an Engineer with the Beijing Institute of Electronic System Engineering. His research interests include dynamics modeling, guidance and control technology, and the controller design of flight vehicles.

YURU BIN was born in Guang'an, Sichuan, in 1999. She received the B.S. degree from the Beijing Institute of Technology, in 2021, where is currently pursuing the degree with the School of Aerospace Engineering.

Her main research interests include missile guidance and control.

HETING WANG was born in 2000. She received the B.S. degree in weapon launch engineering from the Nanjing University of Science and Technology, in 2022. She is currently pursuing the M.S. degree with the Beijing Institute of Technology.

Her research interests include flying vehicle guidance and control technology.

KEQING GUO was born in Changchun, Jilin, in 2001. She received the B.S. degree in aircraft control and information engineering from Sichuan University, Chengdu, China, in 2022. She is currently pursuing the M.S. degree with the Beijing Institute of Technology.

Her research interests include autonomous trajectory planning of flight vehicles and convex optimization and its applications.